Electronic Supplementary Information for:

Unexpected Suppression of Spin-Lattice Relaxation via High Magnetic Field in a High-Spin Iron(III) Complex

Joseph M. Zadrozny,[a] Michael J. Graham,[a] Matthew D. Krzyaniak,[a,b] Michael R. Wasielewski,[a,b] and Danna Freedman.[a,*]

[a]Department of Chemistry, Northwestern University, Evanston, IL, 60208, USA.
[b]Argonne-Northwestern Solar Energy Research (ANSER) Center, Northwestern University, Evanston, IL, 60208, USA.

Chem. Commun.

Table of Contents

Experimental Details.

Sample Preparations and General Considerations.

$(Ph_4P)_3[Fe(C_5O_5)_3]$ and $(Ph_4P)_3[Ga(C_5O_5)_3]$, were prepared according to literature procedure.[1] Samples were handled in air unless otherwise stated.

$(Ph_4P)_3[Fe_{0.001}Ga_{0.999}(C_5O_5)_3]$ (1a) This sample was prepared following literature procedure.[1b]

Electron Paramagnetic Resonance Measurements. Solid samples were generally prepared under ambient atmospheres and polycrystalline samples were finely ground prior to loading into sample tubes (Wilmad, X and Q-band tubes; Vitrocom, W-band) and restrained with molten eicosane. Variable concentrations of dilution were tested; 1:500, 1:1000, and 1:2000 Fe:Ga molar ratios. An enhancement of T_2 was seen at 1:1000 versus 1:500,[1b] but no change was detected between 1:1000 and 1:2000. We thus selected the 1:1000 as the concentration of interest owing to the balance between adequate dilution and the desire for a strong spectroscopic signal. Solutions in SO_2 were prepared as follows. First, a known volume of a given concentration of $(Ph_4P)_3[Fe(C_5O_5)_3]$ in dichloromethane was placed into an X or W-band tube. The tube was then hooked up to a schlenk line and carefully evacuated to remove the solvent without bumping the solution up the walls of the tube. Then, an equal volume of SO_2 (Anhydrous, 99.995 %, Airgas) was condensed into the tube by partial immersion of the end of the EPR tube in liquid N_2. The tube was then flame sealed under vacuum. The tube was allowed to warm briefly at –42 °C in an acetonitrile/dry ice bath to anneal the frozen SO_2 solvent before freezing and storage in liquid nitrogen until analysis. **CAUTION! SO_2 has a boiling point of –10 °C and is a gas at room temperature. While we did not experience any rupturing of EPR tubes after allowing a sample to warm, proper eye protection is required while handling these samples.** Care was taken not to permit long exposure of the sample to room temperature owing to decomposition of **1** into a colorless, EPR-silent species.

Pulsed and Continuous-Wave EPR Measurements. EPR measurements at X and W band were collected on a Bruker Elexsys E680-X/W spectrometer equipped with a split ring resonator (ER4118X-MS5) at X-Band and a cylindrical resonator (EN-680-1021H) at W-band. Pulsed experiments at X-band utilized a 1kW TWT amplifier (Applied Systems Engineering 117X) to generate high-power microwave pulses. The resonator was partially overcoupled to maximize echo intensity and minimize ringdown following application of the microwave pulses. K_a-band EPR measurements were collected on a homebuilt instrument utilizing a custom designed Microwave Bridge from Millitech Inc. Temperature was controlled at $X/K_a/W$ bands with Oxford Instruments CF helium cryostats and an Oxford Instruments ITC503 temperature controller.

T_2 measurements were performed using a two-pulse spin echo sequence, $^{\pi}/_2$-τ-π-τ-*echo*, where τ is the time delay between pulses and π/2 or π denote microwave pulses, nominally 16 and 32 ns in length at X-band, 20 and 40 ns at K_a-band and 132 and 260 ns at W-band. Spin lattice relaxation parameters are influenced by the experimental conditions under which they are obtained. One important influence is spectral diffusion, which can convolute data analysis and obscure the true value of T_1 for a given spin. This effect is commonly observed in the traditional

inversion recovery experiment for obtaining T_1. To eliminate the obscuring effect of spectral diffusion we focused on an alternative pulsed experiment, saturation recovery. This experimental technique is known to relatively minimize the influence of spin diffusion.[2] These T_1 measurements were performed by preceding a two-pulse spin echo sequence with a picket-fence saturation sequence and incrementing the time, T, between the saturation sequence and the echo sequence.

EPR Analysis. Spectral data were processed with Xepr,[3] Origin,[4] Excel,[5] and Matlab.[6] Continuous wave EPR spectra were simulated with Easyspin.[7] Saturation recovery data were normalized and fit with monoexponential recovery functions, $I(t) = 1 - exp\left(-{}^{t}/_{T_1}\right)$, where t is the delay between detection and the saturating pulses and T_1 is the spin-lattice relaxation time, when saturation was complete. When saturation was only partially complete, or when the monoexponential function did not provide a sufficiently good fit, a modified exponential recovery function, $I(t) = 1 - exp\left(-\left({}^{t}/_{T_1} + \sqrt{{}^{t}/_{T1}}\right)\right)$ was used to account for spectral diffusion.[8] We note that the difference in T_1 values between the application of these two functions was minimal and the latter function provided better fits. Coherence times (T_2 or T_m) were determined via fitting the normalized data to exponential decay functions. All fitted T_1 and T_2 parameters are tabulated in Tables S1-S2. In the case of X-band measurements, where strong ^{1}H ESEEM is observed, T_2 values are estimated from fits of the maxima of the observed peaks in the modulation. The 360 ns offset in 2τ for the W-band Hahn-echo measurements owes to the required long pulse lengths and low power of the W-band bridge.

Additional Discussion of EPR Spectra Fits and Implications for M_S level mixing. The fits of the cw and echo detected spectra for **1a** are depicted in Figure S1. The dominant transition employed for pulsed studies at a given frequency is the largest intensity one, occurring at 0.17, 1.17, and 3.28 T for X-, K_a-, and W-band measurements. The g, D, and E values used to fit each frequency are nearly constant, with values of g_x = 2.03(2), g_y = 2.02(2), g_z = 2.02(3), D = –0.29(2) cm^{-1} and $|E|$ = 0.067(3) cm^{-1}. These values enable computing the relative composition of the wavefunctions of the EPR transition as a function of field. We note that uncertainty surrounding the sign of E obtained from the CW analysis propagates to the computed contributions of different M_S levels to those involved in the probed EPR transition. Nevertheless, the foregoing values, assuming positive E, suggest that the ground (nominally $M_S = -{}^1/_2$) and excited (nominally $M_S = +{}^1/_2$) levels for the probed transition are approximately as follows (computed from Matlab) These wavefunctions are best intuited from the standpoint of a field applied parallel to the z-axis of the molecule.:

At 0.17 T

ground state = $0.85\left|+{}^3/_2\right\rangle - 0.52\left|-{}^1/_2\right\rangle - 0.68\left|-{}^5/_2\right\rangle$

excited state = $-0.96\left|-{}^3/_2\right\rangle + 0.26\left|+{}^1/_2\right\rangle + 0.12\left|+{}^5/_2\right\rangle$

At 1.17 T

ground state = $-0.17\left|+{}^3/_2\right\rangle + 0.98\left|-{}^1/_2\right\rangle + 0.05\left|-{}^5/_2\right\rangle$

excited state = $-0.10\left|-{}^3/_2\right\rangle - 0.92\left|+{}^1/_2\right\rangle + 0.37\left|+{}^5/_2\right\rangle$

At 3.28 T

ground state = $-0.05\left|+{}^3/_2\right\rangle + 1.00\left|-{}^1/_2\right\rangle + 0.03\left|-{}^5/_2\right\rangle$

excited state = $0.04\left|-{}^3/_2\right\rangle + 1.00\left|+{}^1/_2\right\rangle - 0.05\left|+{}^5/_2\right\rangle$

Additional Discussion of Relaxation Process Modeling:

Definitive determination of the operative relaxation processes in **1** is difficult despite the application of the multifrequency method. Here, we note that getting a good model of the temperature dependence of T_1 can rapidly approach overparameterization, and multiple different combinations of relaxation mechanisms can potential yield high quality fits to the data. Thus, we judiciously narrowed down our relaxation mechanisms for the fits. Here, we found that the optimum fits employed direct and Raman relaxation processes:

$$\frac{1}{T_1} = A_{direct}T + C_{Raman}\left(\frac{T}{\theta_d}\right)^9 J_8\left(\frac{\theta_d}{T}\right) \qquad (1)$$

Here, C_{Raman} is a proportionality constant, T is the temperature, θ_d the Debye temperature, and $J_8\left(\frac{\theta_d}{T}\right) = \int_0^{\theta_d/T} x^8 \frac{e^x}{(e^x-1)^2} dx$ the transport integral. This fit is displayed in the main text and the best fit parameters are given in Table S3. An explanation for the enhancement of the obtained θ_d at higher field is not available at present. Note that utilization of the Raman process alone as depicted in equation (1) was insufficient to model the data. To attempt a more fundamental understanding for the unusual field dependence of T_1 we also tried to model the data with other field-dependent mechanisms. A combination of a direct process with an Orbach process was also fit to the data, as the latter process can enhance T_1 with increasing field (see Fig. S8).[9] Here, we utilized the contribution of the Orbach process to T_1: $1/T_1 = \tau_0^{-1}\exp(-U_{\text{eff}}/k_B T)$, where τ_0 is the preexponential factor for Orbach relaxation, k_B is the Boltzmann constant, T the temperature, and U_{eff} is the activation energy for relaxation. In our fitting attempts we first set the values of U_{eff} to those that are reasonable based on the Zeeman diagrams (ranging from 0.6 to 0.8 cm^{-1} at 0.17 T, 1.3 to 2.5 cm^{-1} at 1.17 T, and 3.2 to 6.5 cm^{-1} at 3.28 T), which noticeably diminished the quality of the fit. Indeed, refinement of the two processes together with these U_{eff} values consistently eliminated the contribution of the Orbach process despite multiple different initial parameter sets. These observations suggest that such fit results are not merely a local minimum. Separately, we attempted to use a combination of the direct and Orbach processes to model the data (Fig. S7) wherein the value of U_{eff} was allowed to freely refine. Yet, the results of these fits visibly led to lower quality fits than the direct and Raman combination. Further, these fits provided activation energies that are an order of magnitude higher than expected given our knowledge of the M_S level energies for **1** (Fig. S8). The aggregate of these data lend further credence to the analysis provided in the main text.

Table S1. Spin-lattice relaxation times (T_1) obtained on **1a** and **1b** at varying fields and frequencies.

1a	
X-band (9.5 GHz)	
Temp.	T_1 (μs)
4.2	11.2(2)
5	8.4(2)
7	4.8(1)
9	3.0(1)
10	2.6(1)
12	1.83(4)
14	1.58(5)
16	1.31(4)
18	0.81(2)
20	0.70(2)
25	0.32(1)
30	0.25(1)

K_a-band (34 GHz)	
Temp.	T_1 (μs)
5	18.9(7)
7	11.6(4)
9	7.6(3)
10	6.5(3)
12	4.5(2)
14	3.0(2)
16	2.8(1)
18	2.2(1)
20	1.7(2)
25	0.83(9)

W-band (94 GHz)	
Temp.	T_1 (μs)
5	5990(473)
7	3860(163)
9	2460(66)
10	2140(64)
12	1380(36)
14	924(30)
16	612(16)
18	466(15)
20	329(14)
25	172(7)
30	107(5)
35	63(4)
40	41(2)

1b	
X-band (9.5 GHz)	
Temp.	T_1 (μs)
4.2	4.83(9)
5	5.74(15)
7	4.75(17)
9	2.56(8)
12	1.50(4)
14	0.93(3)

W-band (94 GHz)	
Temp.	T_1 (μs)
5	4610(297)
7	3660(156)
9	2670(95)
10	2310(85)
12	1500(47)
14	1070(30)
16	590(16)
18	520(15)
20	390(11)
25	217(8)
30	126(6)
35	84(5)
40	56(4)

Table S2. Spin-spin relaxation times (T_2) obtained on **1a** and **1b** at varying fields and frequencies.

1a	
X-band (9.5 GHz)	
Temp.	T_2 (ns)
4.2	560(19)
5	507(12)
7	416(9)
9	372(9)
10	329(8)
12	296(6)
14	230(5)
16	218(5)
18	200(5)
20	238(6)
25	194(7)
30	151(7)
W-band (94 GHz)	
Temp.	T_2 (ns)
5	1630(21)
7	1391(7)
9	1287(4)
10	1262(4)
12	1216(4)
14	1175(8)
16	1107(5)
18	1040(6)
20	976(6)
25	805(6)
30	665(9)
35	544(10)
40	498(12)

1b	
X-band (9.5 GHz)	
Temp.	T_2 (ns)
4.2	667(8)
5	478(8)
7	344(6)
9	285(6)
10	268(5)
12	242(4)
14	201(4)
W-band (94 GHz)	
Temp.	T_2 (ns)
5	1623(13)
7	1415(12)
9	1296(7)
10	1262(7)
12	1195(5)
14	1135(4)
16	1087(4)
18	1018(3)
20	956(3)
25	832(3)
30	685(3)
35	573(3)
40	498(5)

Table S3. Fit parameters for variable temperature and frequency $1/T_1$ data.

Raman and direct processes				
Field (T)	Frequency (GHz)	A_{direct} ($s^{-1}K^{-1}$)[a]	C_{Raman} ($s^{-1}K^{-9}$)	θ_d (K)
0.17	9.5	$2.3(3) \times 10^4$	$5(3) \times 10^7$	41(11)
1.17	34	$1.1(1) \times 10^4$	$2(1) \times 10^7$	47(12)
3.28	94	37(2)	$8(1) \times 10^5$	82(5)

Direct and Orbach Processes				
Field (T)	Frequency (GHz)	c_1 ($s^{-1}K^{-1}$)	τ_0 (s^{-1})	U_{eff} (cm^{-1})
0.17	9.5	$2.9(8) \times 10^5$	$2.8(7) \times 10^{-8}$	49(6)
1.17	34	$1.7(2) \times 10^5$	$2(1) \times 10^{-8}$	71(9)
3.28	94	82(11)	$2.1(3) \times 10^{-6}$	87(5)

[a]Fixed for the purposes of fitting.

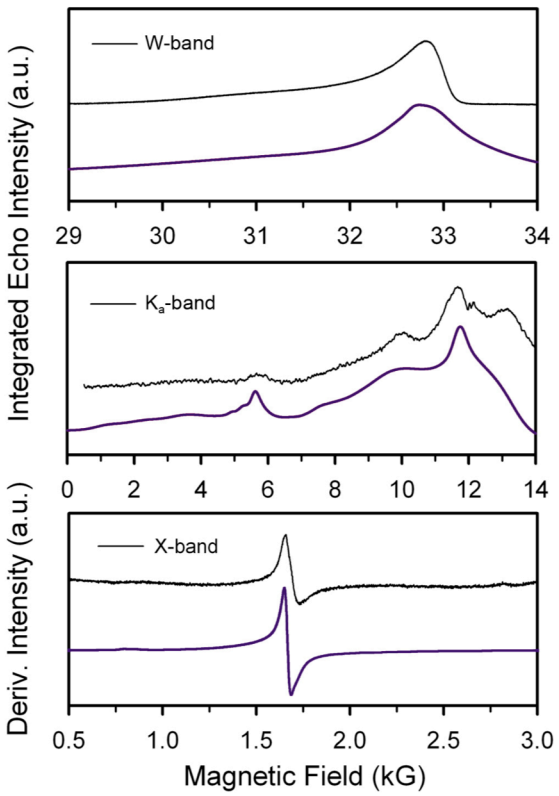

Figure S1. Echo detected (top two panels) and continuous wave (lower panel) EPR spectra at 10 K for **1a** at the indicated frequencies. Parameters for collection of the echo detected spectra are as follows: K_a-band, $^{\pi}/_2$ and π pulses of 20 and 40 ns respectively, with 220 ns interpulse spacing; W-band, $^{\pi}/_2$ and π pulses of 132 and 260 ns respectively with 360 ns interpulse delay. Purple lines are simulated spectra from Easyspin using the parameters $g_x = 2.03(2)$, $g_y = 2.02(2)$, $g_z = 2.02(3)$, $D = -0.29(2)$ cm^{-1} and $|E| = 0.067(3)$ cm^{-1}. These values reflect those from previously published high-frequency experiments.[1b] D strain was used to model broadening in the spectra that occurs from slight variation in the coordination geometry across the powder. For X-, K_a-, and W-band the applied strains were [4800 2000], [3800 1000], and [7000 1000]. CW and Echo detected spectra for $(Ph_4P)_3[Fe(C_5O_5)_3]$, can also be found in Ref. 1b.

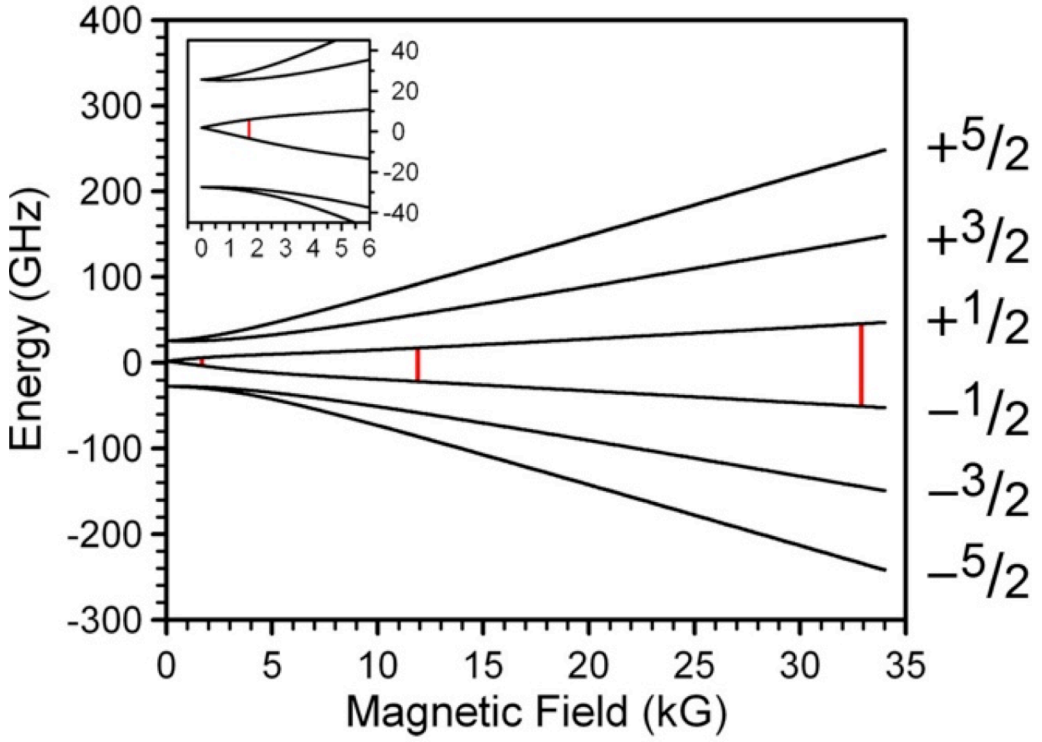

Figure S2. Energies of the M_S levels as a function of applied dc magnetic field perpendicular to the molecule for **1**. Energies were calculated with Easyspin and the parameters provided in the caption of Figure S1. Red vertical lines indicate the transitions investigated in this manuscript at X-, K_a-, and W-band. The M_S levels are individually labeled by those appropriate in the high-field limit. The inset is a magnification of the low-field region for clarity regarding the X-band resonance.

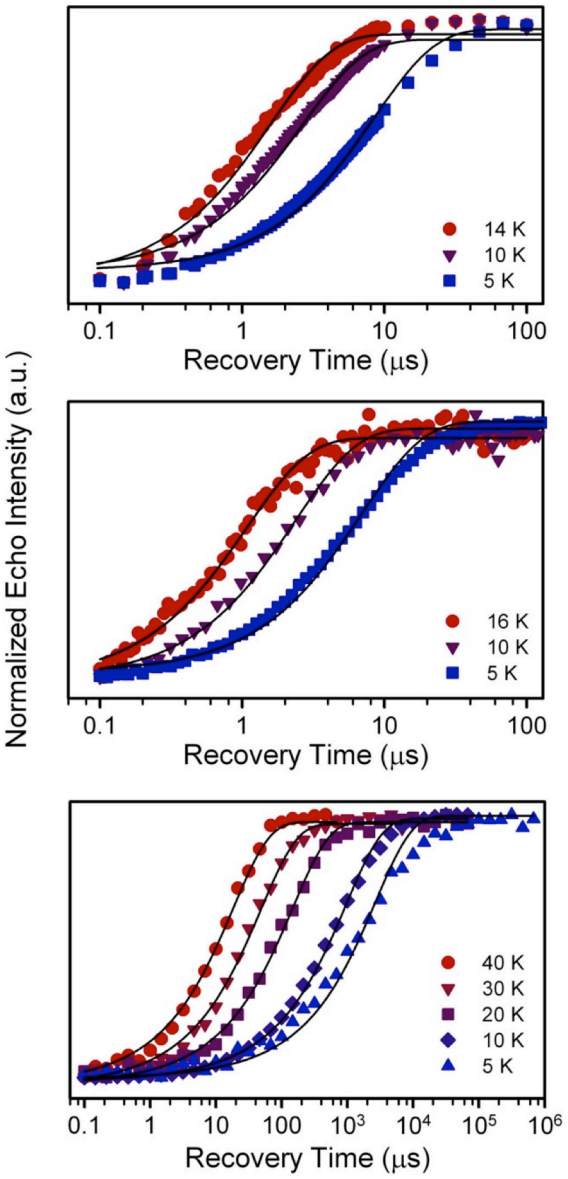

Figure S3. Select saturation recovery curves for **1a** at X-band (top) K_a-band (middle) and W-band (bottom) at the indicated temperatures. Black lines indicate best fits to exponential recovery functions. Specific fitted parameters are tabulated in Table S1. Saturation recovery pulse sequence information is given in the experimental details above.

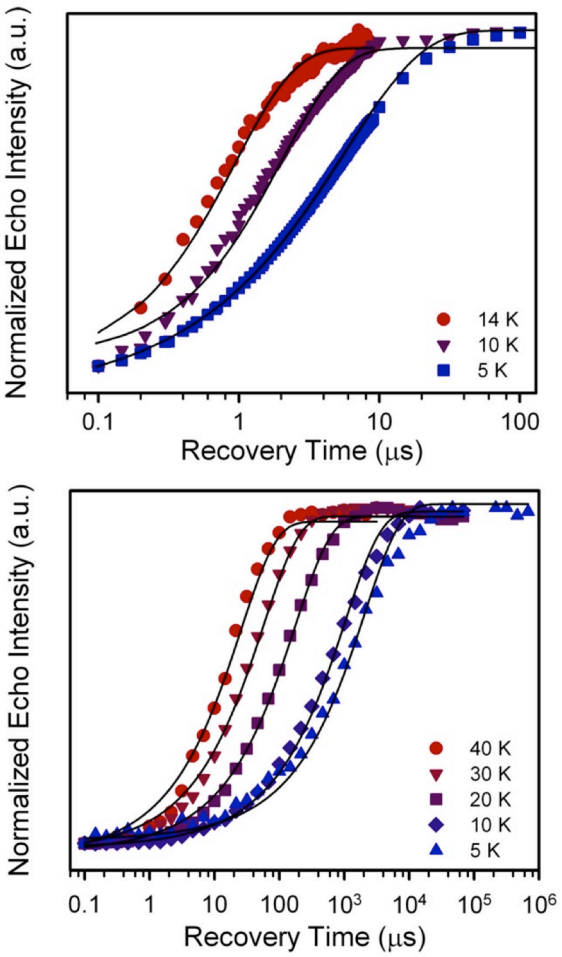

Figure S4. Select saturation recovery curves for **1b** at X-band (top) and W-band (bottom) at the indicated temperatures. Black lines indicate best fits to exponential recovery functions. Fitted parameters can be found in Table S1. Saturation recovery pulse sequence information is provided in the experimental details above.

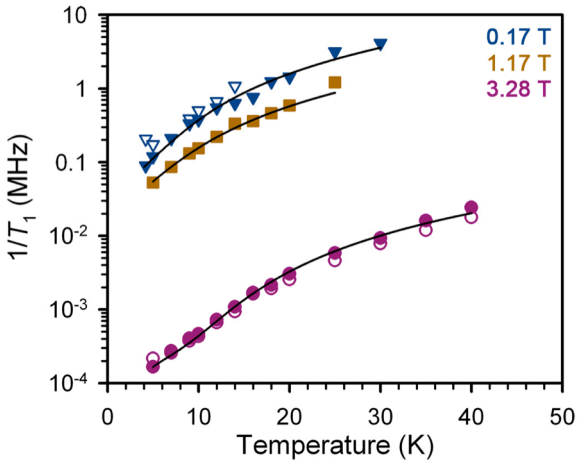

Figure S5. Temperature dependence of the spin-lattice relaxation time T_1 for **1a** (filled symbols) and **1b** (empty symbols). Black lines represent best fits to the data that account for spin-lattice relaxation via direct and Raman processes. These data are provided as $1/T_1$ as a guide to considering these phenomena through the lens of comparing rates.

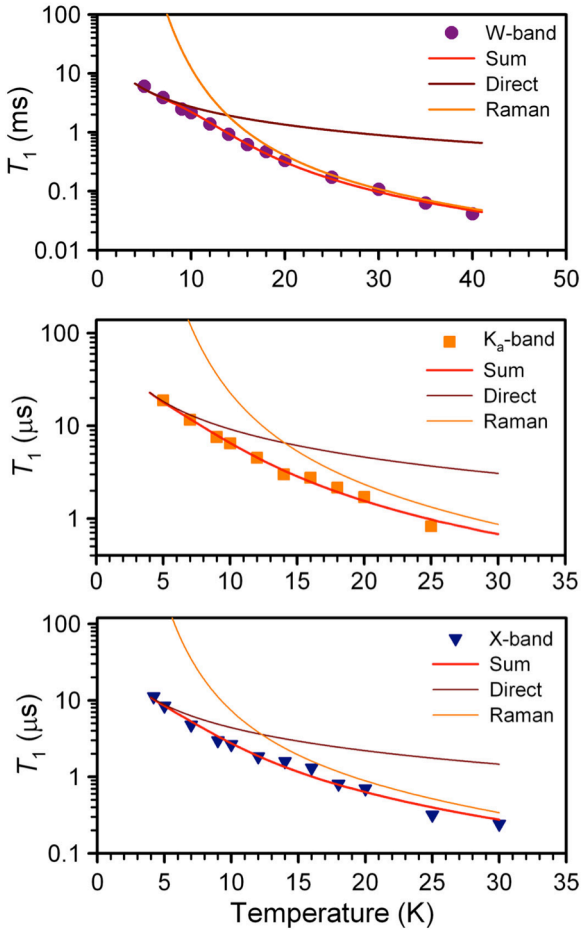

Figure S6. Variable-temperature T_1 data for **1a** at W- (top), K_a- (middle), and X-band (bottom). Red lines represent the best fits to the data as a sum of direct and Raman processes, with the individual contributions of the two relaxation processes highlighted. The equation for modeling T_1 is given in the discussion at the beginning of the ESI. The best fit parameters for each frequency are provided in Table S3.

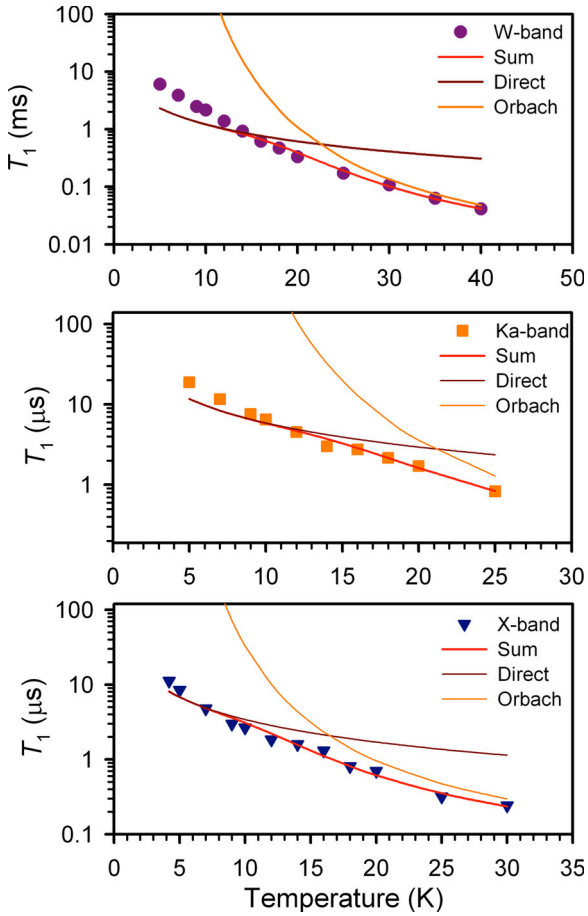

Figure S7. Variable-temperature T_1 data fits for **1a** as sums of direct and Orbach processes. The individual contributions of the two relaxation processes are highlighted. The equation for modeling is $1/T_1 = A_{\text{direct}}T + \tau_0\exp(-U_{eff}/k_BT)$, where A_{direct} is the coefficient for the direct process, T the temperature, and the second term is for the Orbach process with parameters defined in the extended discussion at the beginning of the ESI. The best fit parameters for these processes are given in Table S3.

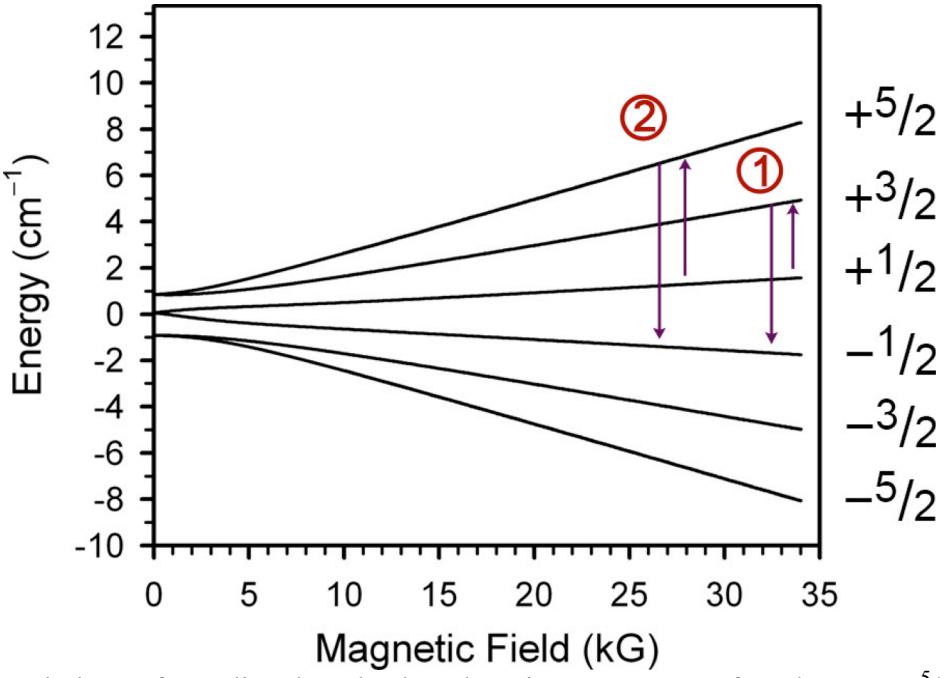

Figure S8. Depiction of predicted Orbach relaxation processes for the $S = {}^{5}/_{2}$ moment of $[Fe(C_5O_5)_3]^{3-}$. For both pathways initial excitation to an excited state is required before relaxation to the ground state. For the pathway designated as **1**, this excitation is to the nearest level, while for **2** it is to the next nearest level. Note that this activation energy decreases with decreasing field. Use of these activation energies for the Orbach process fits produced significantly worse quality fits. For the fits in Figure S7, the obtained Orbach processes corresponded to U_{eff} values that were unreasonably higher than the expected values as depicted in this figure.

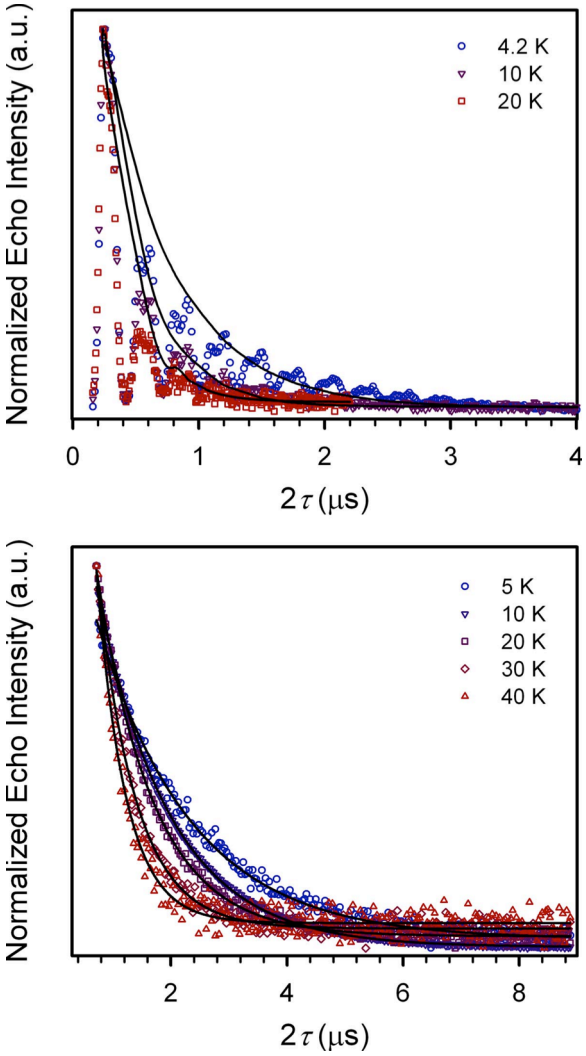

Figure S9. Select variable temperature echo decay curves for **1a** at X and W-band. Pulse sequences utilized 16 and 32 ns π and $^{\pi}/_{2}$ pulse lengths for X-band and 132 and 260 ns π and $^{\pi}/_{2}$ pulse lengths for W-band, respectively. Fitted parameters can be found in Table S2.

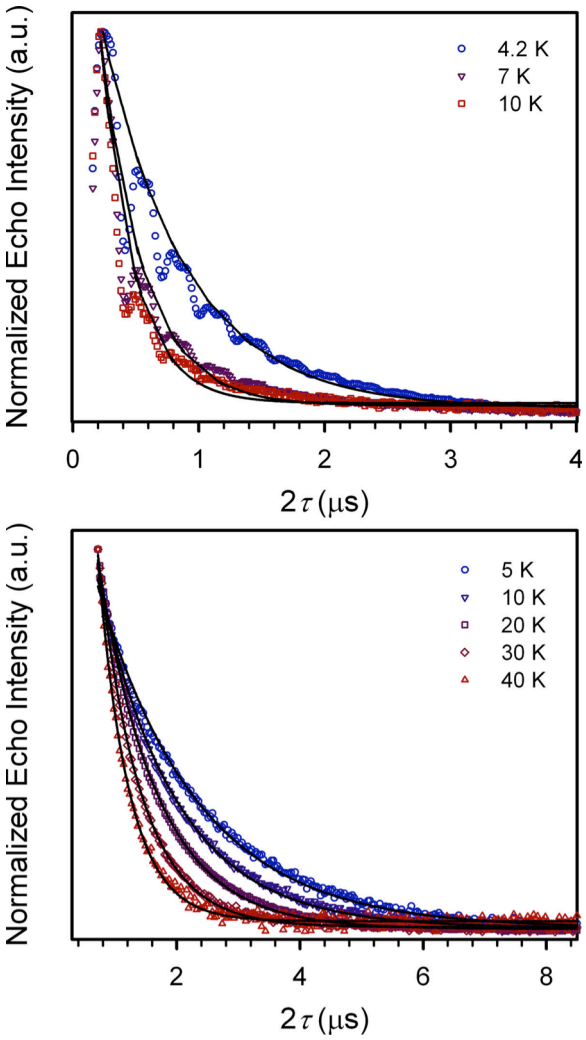

Figure S10. Select variable temperature echo decay curves for **1b** at X and W-band. Pulse sequences utilized 16 and 32 ns π and $^{\pi}/_{2}$ pulse lengths for X-band and 132 and 260 ns π and $^{\pi}/_{2}$ pulse lengths for W-band, respectively. Fitted parameters can be found in Table S2.

References

1. (*a*) S. Curreli, P. Deplano, C. Faulmann, M. L. Mercuri, L. Pilia, A. Serpe, E. Coronado and C. J. Gómez-García, *Inorg. Chim. Acta.* 2006, **359**, 1177-1183. (*b*) J. M. Zadrozny and D. E. Freedman *Inorg. Chem.* 2015, **54**, 12027-12031.
2. A. Schweiger and G. Jeschke, *Principles of pulse electron paramagnetic resonance*, Oxford University Press, New York, 2001.
3. Xepr; Bruker Biospin, Billerica, MA, United States.
4. Origin; OriginLab, Northampton, MA, United States.
5. Microsoft Excel; Microsoft, Redmond, WA, United States.
6. Matlab 12b; The MathWorks, Inc., Natick, MA, United States.
7. S. Stoll and A. Schweiger, *J. Magn. Reson.* 2006, **178**, 42-55.
8. R. Boscaino, F. M. Gelardi and R. N. Mantegna, *Phys. Lett.* 1984, **103A**, 391-393.
9. C. B. P. Finn, R. Orbach and W. P. Wolf, *Proc. Phys. Soc.* 1961, **77**, 261-268.